

Complex trajectory method in time-dependent WKB

Yair Goldfarb¹, Jeremy Schiff^{1,2,3} and David J. Tannor¹

¹*Department of Chemical Physics,*

²*Department of Mathematics,*

The Weizmann Institute of Science,

Rehovot, 76100 Israel

November 1, 2018

Abstract

We present a significant improvement to a time-dependent WKB (TDWKB) formulation developed by Boiron and Lombardi [JCP **108**, 3431 (1998)] in which the TDWKB equations are solved along classical trajectories that propagate in the complex plane. Boiron and Lombardi showed that the method gives very good agreement with the exact quantum mechanical result as long as the wavefunction does not exhibit interference effects such as oscillations and nodes. In this paper we show that this limitation can be overcome by superposing the contributions of *crossing* trajectories. We also demonstrate that the approximation improves when incorporating higher order terms in the expansion. These improvements could make the TDWKB formulation a competitive alternative to current time-dependent semiclassical methods.

³On sabbatical leave from Dept. of Mathematics, Bar-Ilan University, Ramat Gan 52900, Israel.

PACS numbers:

I. INTRODUCTION

The difficulty in performing quantum mechanical calculations of multi-dimensional systems has stimulated an intensive and ongoing effort in the last three decades to develop numerical tools based on semiclassical mechanics. In this context, we refer to semiclassical mechanics as the derivation of a quantum mechanical wavefunction or propagator via propagation of classical (or classical-like) trajectories. From a physical point of view, semiclassical methods try to evade the non-locality imbedded in quantum mechanics. Mathematically speaking, semiclassical methods aim at casting the time-dependent Schrödinger equation (TDSE), which is a PDE, in terms of ODEs related to classical equations of motion. This transformation has significant computational advantages that can ease the inherent difficulty of multi-dimensional quantum calculations.

The WKB method[1, 2, 3] can be considered as the first of the semiclassical methods. Its date of birth almost coincides with the publication of the Schrödinger equation in 1926, and virtually every standard text book in quantum mechanics has a description of the method. The basic idea of the WKB method is to recast the wavefunction as the exponential of a function and then replace the exponent with a power series in \hbar . The WKB method is ordinarily applied to the *time-independent* Schrödinger equation and provides for a good approximation to the eigenstates as long as one is not too near a classical turning point. It is only natural that as part of the effort to develop time-dependent semiclassical methods, a time-dependent version of the WKB method would be explored. Surprisingly little work has been done in this direction[4, 5, 6, 7, 8, 9, 10, 11, 12, 13, 14, 15, 16]. A decade ago, Boiron and Lombardi[17] developed a complex trajectory version of time-dependent WKB (TDWKB), which we refer to as CTDWKB. In conventional WKB the leading order term in the phase of the wave function is taken to be $O(\hbar^{-1})$ and the leading order term in the amplitude is taken to be $O(\hbar^0)$. In contrast, the CTDWKB formulation treats the amplitude and phase on an equal footing. The price to pay for this procedure is that the resulting classical trajectories propagate in the complex plane. The benefits are that the results are superior to standard TDWKB and no singularities are encountered during the integration of the equation of motion.

The CTDWKB equations of motion can be solved analytically and yield the *exact* wavefunction for an initial Gaussian wavepacket in a potential with up to quadratic terms. The

first-order method was tested numerically by Boiron and Lombardi for scattering of a Gaussian wavepacket from a potential barrier. They showed that the method produced very good results as long as the wavefunction did not exhibit *interference effects* in the form of oscillations or nodes[17]. In this paper we present a simple modification to CTDWKB that provides an accurate description of oscillations in the wavefunction. We show that complex classical trajectories, similar to real classical trajectories, can cross in configuration space. By superposing the contributions from two or more crossing trajectories, interference effects are obtained. We take CTDWKB a step further in another direction by showing that the approximation generally improves when incorporating additional terms in the series expansion. Since the WKB expansion is an asymptotic series, this observation is non-trivial.

Two other semiclassical formulations that incorporate complex trajectories should be mentioned in relation with CTDWKB. The first is the Generalized Gaussian Wavepacket Dynamics (GGWPD) developed by Huber, Heller and Littlejohn [18, 19]. One may show that for an initial Gaussian wavepacket the equations of motion of GGWPD are de facto identical to the equations of the first-order approximation of CTDWKB. However the GGWPD has no generalization to arbitrary initial wavefunctions and no systematic way to increase the accuracy of the approximation. On the other hand, in reference [18], Huber and Heller appreciate the importance of multiple complex trajectories in obtaining interference phenomena. Here we incorporate the idea of crossing complex trajectories into the more general CTDWKB formulation.

The second formulation that is closely related to CTDWKB is Bohmian Mechanics with Complex Action (BOMCA)[20, 21]. CTDWKB and BOMCA begin with the same ansatz of substituting of an exponential function $\exp[iS/\hbar]$ into the TDSE. Similar to CTDWKB, the BOMCA formulation incorporates equations of motion that propagate along complex trajectories. The first-order equations of motion of BOMCA are identical to the equations of first-order CTDWKB. The differences between the two formulations are: (1) The equations of motion in BOMCA are for the coefficients of spatial derivatives of the phase. In CTDWKB the equations of motion are for the coefficients of an \hbar Taylor expansion of the phase and their spatial derivatives. (2) Incorporating higher order terms of the CTDWKB approximation does not effect the the results for lower order terms since each equation of motion depends only on lower terms of the expansion. This is not the case with BOMCA where each equation of motion depends on both lower and higher terms resulting in a backward feedback. (3) A

result of the last difference is that in CTDWKB the equations of motion of the trajectories remain *classical* whereas in BOMCA, the inclusion of higher orders of the approximation affect the complex trajectories by adding a “quantum force” that yields *quantum* trajectories.

This paper is organized as follows. In section II we formulate TDWKB and the CTDWKB. Our derivation is more compact than the Boiron-Lombardi derivation and demonstrates how to obtain the equations of motion for higher orders of the expansion in a simple manner. In Section III we apply the formulation to a Gaussian initial wavepacket propagating in a quartic double-well potential. We demonstrate that superimposing the contributions of crossing trajectories leads to interference effects and that incorporating higher order terms in the expansion improves the approximation. Section IV is a summary and concluding remarks. Following Boiron and Lombardi we will refer to the CTDWKB method in the body of the paper as the complex trajectory method (CTM) for short.

II. FORMULATION

A. Time-independent vs. Time-dependent WKB

For simplicity we present the one-dimensional version of the CTM derivation. The generalization to multi-dimensions can be performed in a straightforward manner. The conventional WKB derivation begins by inserting the ansatz

$$\psi(x) = \exp \left[\frac{i}{\hbar} S(x) \right], \quad (2.1)$$

into the *time-independent* Schrödinger equation, where \hbar is Planck’s constant divided by 2π . The end result is

$$\frac{1}{2m} \left(\frac{dS}{dx} \right)^2 + V(x) - \frac{i\hbar}{2m} \frac{d^2S}{dx^2} = E, \quad (2.2)$$

where m is the mass of the particle, $V(x)$ is the potential energy and E is the eigenvalue. If we assume that $S(x)$ can be expanded asymptotically as a polynomial in \hbar

$$S(x) = S_0(x) + \hbar S_1(x) + \hbar^2 S_2(x) + \dots = \sum_{j=0}^{\infty} \hbar^j S_j(x), \quad (2.3)$$

then, by substituting the last equation into eq.(2.2) and equating powers of \hbar , a series of coupled ODEs are obtained for the S_j ’s.

The time-dependent WKB begins by inserting the ansatz[4, 5]

$$\psi(x, t) = \exp \left[\frac{i}{\hbar} S(x, t) \right], \quad (2.4)$$

into the time-dependent Schrödinger equation,

$$i\hbar\partial_t\psi = -\frac{\hbar^2}{2m}\partial_{xx}\psi + V(x, t)\psi, \quad (2.5)$$

The result is the quantum Hamilton-Jacobi equation[4, 5]

$$\partial_t S + \frac{1}{2m}(\partial_x S)^2 + V = \frac{i\hbar}{2m}\partial_{xx}S, \quad (2.6)$$

where the LHS of the equation is in the form of the classical Hamilton-Jacobi equation. Equation (2.6) is formally exact since no approximation has been introduced. In TDWKB formulation we insert into eq.(2.6) a time-dependent version of eq.(2.3)

$$S(x, t) = \sum_{j=0}^{\infty} \hbar^j S_j(x, t). \quad (2.7)$$

The result is

$$\sum_{j=0}^{\infty} \hbar^j \partial_t S_j + \frac{1}{2m} \sum_{j_1, j_2=0}^{\infty} \hbar^{j_1+j_2} \partial_x S_{j_1} \partial_x S_{j_2} + V = \frac{i}{2m} \sum_{j=0}^{\infty} \hbar^{j+1} \partial_{xx} S_j. \quad (2.8)$$

By equating terms having the same powers of \hbar we obtain the classical Hamilton-Jacobi equation for $S_0(x, t)$

$$\partial_t S_0 + \frac{1}{2m}(\partial_x S_0)^2 + V = 0, \quad (2.9)$$

and equations of motion for $S_n(x, t), n \geq 1$

$$\partial_t S_n + \frac{\partial_x S_0}{m} \partial_x S_n = \frac{i}{2m} \partial_{xx} S_{n-1} - \frac{1}{2m} \sum_{j=1}^{n-1} \partial_x S_j \cdot \partial_x S_{n-j}. \quad (2.10)$$

Conveniently, each equation depends only on lower order terms. The next step in TDWKB is to convert eqs.(2.9) and (2.10) into a set of ODEs by looking at the evolution of S_0, S_1, \dots along classical trajectories, as described in the next section.

B. Integrating along classical trajectories

As we mentioned earlier, the first term in the \hbar power expansion, S_0 , obeys the Hamilton-Jacobi equation (eq.(2.9)). This equation is an alternative formulation of Newton's second

law of motion in terms of an action field. The emergence of classical trajectories in the TDWKB equations provides the incentive to solve eqs.(2.9) and (2.10) by integrating along such trajectories.

The link between the Hamilton-Jacobi equation and classical trajectories is demonstrated by defining the *velocity field*

$$v(x, t) \equiv \frac{\partial_x S_0(x, t)}{m} \quad (2.11)$$

and considering the trajectories defined by

$$\frac{dx}{dt} = v(x, t) . \quad (2.12)$$

By taking the spatial partial derivative of eq.(2.9), using the definition of the Lagrangian time derivative $\frac{d}{dt} \equiv \partial_t + \frac{dx}{dt} \partial_x$, and applying eq.(2.11) we obtain the equation of motion for the velocity along a trajectory as Newton's second law

$$\frac{dv}{dt} = -\frac{\partial_x V}{m} . \quad (2.13)$$

Hence, the trajectories defined are simply classical trajectories.

Inserting eq.(2.9) in the Lagrangian time derivative of S_0 yields

$$\frac{dS_0}{dt} = \partial_t S_0 + \frac{\partial S_0}{m} \partial_x S_0 = \frac{1}{2} m v^2 - V, \quad (2.14)$$

where we recognize the equation of motion for the action along a classical trajectory. Noting that v is a mere dummy variable, we summarize the equations of motion for the zeroth order term of TDWKB, S_0

$$\frac{dx}{dt} = \frac{\partial_x S_0}{m}, \quad (2.15)$$

$$\frac{d(\partial_x S_0)}{dt} = -\partial_x V, \quad (2.16)$$

$$\frac{dS_0}{dt} = \frac{1}{2m} (\partial_x S_0)^2 - V. \quad (2.17)$$

We turn to the higher order terms in the series S_n , $n \geq 1$. Recognizing the LHS of eqs.(2.10) as the Lagrangian time derivative of S_n , we can write

$$\frac{dS_n}{dt} = \frac{i}{2m} \partial_{xx} S_{n-1} - \frac{1}{2m} \sum_{j=1}^{n-1} \partial_x S_j \cdot \partial_x S_{n-j}. \quad (2.18)$$

These equations do not constitute a closed set of ODEs since they depend on partial derivatives such as $\partial_{xx} S_n$. We close the set of equations by deriving equations of motion for the

partial derivatives on the RHS of eq.(2.18) ($\partial_{xx}S_{n-1}$, $\partial_x S_j$ and $\partial_x S_{n-j}$). We demonstrate the process by deriving equations of motion for S_1 and S_2 . Inserting $n = 1$ in eq.(2.18) yields

$$\frac{dS_1}{dt} = \frac{i}{2m}\partial_{xx}S_0. \quad (2.19)$$

An equation of motion for $\partial_{xx}S_0$ is obtained by taking a second spatial partial derivative of eq.(2.9),

$$\partial_{xxt}S_0 + \frac{1}{m} [\partial_x S_0 \cdot \partial_{xxx}S_0 + (\partial_{xx}S_0)^2] + \partial_{xx}V = 0, \quad (2.20)$$

and rewriting it as

$$\frac{d(\partial_{xx}S_0)}{dt} = -\frac{1}{m}(\partial_{xx}S_0)^2 - \partial_{xx}V. \quad (2.21)$$

This equation is derived in reference [17] by a cumbersome finite difference scheme. It is equivalent to eq.(2.9d) of reference [19] where the equation appears in the context of GGWPD. Note that an equation of motion for any order of spatial derivatives of S_0 can be derived in a similar fashion by taking consecutive spatial derivatives of eq.(2.20) and then grouping the Lagrangian time derivative terms. Equations (2.19) and (2.21) provide a closed set of equations of motion for S_1 .

Inserting $n = 2$ into eq.(2.18) yields

$$\frac{dS_2}{dt} = \frac{i}{2m}\partial_{xx}S_1 - \frac{1}{2m}(\partial_x S_1)^2. \quad (2.22)$$

The equations of motion for $\partial_x S_1$ and $\partial_{xx}S_1$ are obtained by first inserting $n = 1$ in eq.(2.10). We then derive two equations by taking a first and a second spatial partial derivative of the result. By grouping the Lagrangian time derivatives of $\partial_x S_1$ and $\partial_{xx}S_1$ in each of the two equations separately we obtain

$$\begin{aligned} \frac{d(\partial_x S_1)}{dt} &= \frac{i}{2m}\partial_{xxx}S_0 - \frac{1}{m}\partial_x S_1 \cdot \partial_{xx}S_0, \\ \frac{d(\partial_{xx}S_1)}{dt} &= \frac{i}{2m}\partial_{xxxx}S_0 - \frac{1}{m}\partial_x S_1 \cdot \partial_{xxx}S_0 - \frac{2}{m}\partial_{xx}S_1 \cdot \partial_{xx}S_0. \end{aligned} \quad (2.23)$$

The last equations depend in turn on $\partial_{xxx}S_0$ and $\partial_{xxxx}S_0$. As mentioned earlier, the equation of motion for these terms can be obtained by additional spatial derivatives of eq.(2.20), a process that yields

$$\begin{aligned} \frac{d(\partial_{xxx}S_0)}{dt} &= -\frac{3}{m}\partial_{xx}S_0 \cdot \partial_{xxx}S_0 - \partial_{xxx}V, \\ \frac{d(\partial_{xxxx}S_0)}{dt} &= -\frac{1}{m} [4\partial_{xx}S_0 \cdot \partial_{xxxx}S_0 - 3(\partial_{xxx}S_0)^2] - \partial_{xxxx}V. \end{aligned} \quad (2.24)$$

Equations (2.21) and (2.22)-(2.24) provide a closed set of equations of motion for S_2 . The scheme we described for S_1 and S_2 can be extended to any of the higher order terms in the expansion. Note that incorporating higher order terms S_n in the TDWKB approximation does not affect the classical trajectories associated with S_0 , defined by eqs.(2.15) and (2.16). We now turn to the source of the distinction between conventional TDWKB and CTM.

C. Initial conditions and complex classical trajectories

In conventional TDWKB the initial wavefunction is “divided” between $S_0(x, 0)$ and $S_1(x, 0)$

$$\psi(x, 0) = A(x) \exp[i\phi(x)] = \exp \left[\frac{i}{\hbar} S_0(x, 0) + S_1(x, 0) \right], \quad (2.25)$$

where $A(x)$ and $\phi(x)$ are the initial amplitude and phase respectively, both taken to be real. The phase is related to the zero-order term S_0 and the amplitude to the first-order correction term S_1 according to

$$S_0(x, 0) = \hbar\phi(x), \quad S_1(x, 0) = -i \ln[A(x)], \quad (2.26)$$

and $S_n(x, 0) = 0$ for $n \geq 2$. Note that the initial conditions specified by eqs.(2.26) yield classical trajectories that propagate on the *real* axis since S_0 and its spatial derivatives are real quantities (see eqs.(2.15) and (2.16)). In contrast, in CTM the amplitude and phase are treated on an equal footing with far-reaching consequences. The initial wavefunction is specified by $S_0(x, 0)$

$$S_0(x, 0) = -i\hbar \ln[\psi(x, 0)], \quad S_n(x, 0) = 0, \quad n \geq 1. \quad (2.27)$$

Since S_0 is generally complex and since the initial velocity $v(x, 0) \equiv \partial_x S_0(x, 0)/m$, the trajectories propagate in the *complex plane* even if the initial positions are on the real axis ($\Im[x(0)] = 0$). This observation requires us to look at the analytic continuation of the wavefunction in the complex plane and find ways to extract the wavefunction on the real axis.

D. Complex root search and superposition

One of the benefits of conventional TDWKB and CTM compared with BOMCA, is that the trajectories obey the classical equations of motion and are independent of the order of the

phase expansion we incorporate in the final wavefunction. But the fact still remains that for an arbitrary initial position $x(0) \in \mathbb{C}$ and an arbitrary final propagation time t_f the final position $x(t_f)$ is complex and yields an “analytically continued” wavefunction at $x(t_f)$

$$\psi[x(t_f), t_f] \approx \exp \left\{ \frac{i}{\hbar} \sum_{j=0}^N \hbar^j S_j[x(t_f), t_f] \right\}, \quad (2.28)$$

where the non-negative integer N is the order of the approximation. References [17, 19, 20] include discussions of root search algorithms for the derivation of initial positions that reach the *real* axis at a given time. We will not describe all the details here but will just state the central idea. The complex root search exploits the assumption that the mapping $x(0) \mapsto x(t_f)$ is analytic. This property allows for an iterative process that detects the initial positions that correspond to real final positions. As demonstrated in references [18, 19] and in section III A, for an arbitrary potential and final time, the mapping is only *locally* analytic. Generally, more than one initial position ends at a final position (whether real or complex). This makes the search for trajectories that end on the real axis more complicated but it has an important advantage in terms of interference effects.

Our main observation is that the contribution of multiple trajectories in CTM can accumulate to an interference pattern. For simplicity we make the following assumption. Suppose that L trajectories end at final time t_f on real position $x(t_f)$. Then the final wavefunction is approximated by a superposition of contributions

$$\psi[x(t_f), t_f] \approx \sum_{l=1}^L \exp \left\{ \frac{i}{\hbar} S^l[x(t_f), t_f] \right\}, \quad (2.29)$$

where each trajectory (denoted by the index l) is associated with a phase $S^l[x(t_f), t_f]$

$$S^l[x(t_f), t_f] = \sum_{j=0}^N \hbar^j S_j^l[x(t_f), t_f], \quad (2.30)$$

that is calculated by the CTM equations of motion. In section III we show that this assumption is too simplified and does not hold at all times and all positions. For example, for positions associated with a tunneling part of the wavefunction, only one of the multiple trajectories should be taken into account. A partial discussion on the superposition of contributions from complex trajectories appears in reference [19] in the GGWPD context. In a forthcoming paper [22] we will explain an alternative derivation of the CTM in which the need to include multiple trajectories for certain times and positions becomes apparent

III. NUMERICAL RESULTS

In this section we examine numerically the CTM formulation allowing for the superposition of complex trajectories. For ready comparison the physical system we choose is identical to the one studied by Boiron and Lombardi (reference [17] section IVB). The potential considered is a quartic double-well

$$V(x) = 1.25 \times 10^{-4}(x^4 - 400x^2). \quad (3.1)$$

The initial wavefunction is a Gaussian wavepacket

$$\psi(x, 0) = \exp \left[-\alpha_0(x - x_c)^2 + \frac{i}{\hbar} p_c(x - x_c) + \frac{i}{\hbar} \gamma_0 \right], \quad (3.2)$$

where $\alpha_0 = 1$, $x_c = 0$, $p_c = 5$, $\gamma_0 = -\frac{i\hbar}{4} \ln(\frac{2\alpha_0}{\pi})$ and we take $m = \hbar = 1$ (all quantities are given in atomic units). The initial conditions for the terms in the \hbar power-expansion of the phase are

$$S_0(x, 0) = i\alpha_0\hbar(x - x_c)^2 + p_c(x - x_c) + \gamma_0 = ix^2 + 5x + \gamma_0, \quad (3.3)$$

$$\partial_x S_0(x, 0) = 2i\alpha_0\hbar(x - x_c) + p_c = 2ix + 5, \quad (3.4)$$

$$\partial_{xx} S_0(x, 0) = 2i\alpha_0\hbar = 2i, \quad (3.5)$$

$$\partial_x^j S_0(x, 0) = 0, \quad j \geq 3, \quad (3.6)$$

$$\partial_x^j S_k(x, 0) = 0, \quad j \geq 0, \quad k \geq 1, \quad (3.7)$$

where $\partial_x^j S_k \equiv \frac{\partial^j S_k}{\partial x^j}$.

In section III A we analyze the first order approximation of CTM ($N = 1$, $S = S_0 + \hbar S_1$) and the properties of the trajectories. Section III B is dedicated to the next order of the approximation ($N = 2$, $S = S_0 + \hbar S_1 + \hbar^2 S_2$). We omit an analysis of $N = 0$ since it is well presented in reference [17] and only yields poor results.

A. First Order approximation, $N = 1$

The first order approximation of CTM requires the solution of eqs.(2.15), (2.16), (2.17), (2.19) and (2.21). The first two equations define the complex classical trajectories and the next three equations yield S_0 and S_1 . We start by analyzing the complex classical trajectories. As mentioned above, the mapping $x(0) \mapsto x(t_f)$ is not one-to-one. For the quartic

potential, we found that three initial positions are mapped to every real final position at $t_f > 0$. For short time scales this observation can be supported analytically. For general potentials or for longer time scales than we present here, more than three initial positions might lead to the same final position[19, 21]. In figures 1(a) and 1(b) we plot complex classical trajectories for $t_f = 3$ and $t_f = 6$ respectively. The *initial positions* of the trajectories can be divided into three groups referred to as *branches*[19]. One group of the initial positions is called the real branch and the other groups are called the secondary branches. The real branch is characterized by the property that it includes the initial position of a trajectory that propagates *solely* on the real axis. We refer to this trajectory as the real trajectory. It can be readily verified that for a Gaussian initial wavefunction there is only a single real trajectory that initiates at $x(0) = x_c$ (see eqs.(2.16), eq.(2.15) and (3.4)). In fig.1(b) we depict the real trajectory explicitly. The secondary branches are defined simply as the groups of initial positions that do not belong to the real branch. Generally, the branches might be infinitely long curves in the complex plane. We will use the term branches to refer to the locus of *initial* positions that leads to final positions where the wavefunction is significantly different from zero. Hence, the branches are curves of *finite* length in the complex plane, although clearly there is some arbitrariness to their length.

In fig.1(a) we see that at short time scales the secondary branches are centered far from neighborhood of the real axis. We can show analytically that for small times t_f the initial positions that comprise the real branch obey $|x(0)| = O(t_f)$ whereas the secondary branches obey $|x(0)| = O(\frac{1}{t_f})$. Note that the linear dependence of the initial momentum on position (eq.(3.4)) allows trajectories with initial positions far from the real axis to reach a real final position in a short time. Unlike the secondary branches, the real branch is centered in the vicinity of the real axis at all times. The initial position $x(0) = x_c$ is a fixed point of the real branch and prevents the real branch (recall that this is the locus of *initial* positions) from “straying” from the neighborhood of the real axis as the final time t_f is increased. At intermediate times (time scales comparable to the time of the collision of the wavefunction with the barrier, $4 \lesssim t_f \lesssim 7$) secondary branch (1) reaches the vicinity of the real axis (fig.1(b)) and at longer time scales it continues in the direction of the positive imaginary axis. As we demonstrate below, the proximity of secondary branch (1) to the real axis is closely related to the size of its contribution to the final form of the wavefunction and its role in interference effects. Secondary branch (2) does not reach the vicinity of the real axis

for any of the time scales specified below. The contribution of this branch to the absolute value of the final wavefunction (eq.(2.29)) is negligible (in the order of 10^{-35}). Hence, from here on we ignore secondary branch (2) and refer to secondary branch (1) as *the* secondary branch.

As we mentioned in section IID, the existence of more than one branch motivates the attempt to superpose the contributions of the real branch and secondary branch in the final wavefunction

$$\psi[x(t_f), t_f] = \psi_R + \psi_S; \quad \psi_R = \exp\left[\frac{i}{\hbar}S_{\text{Real}}\right], \quad \psi_S = \exp\left[\frac{i}{\hbar}S_{\text{Sec}}\right], \quad (3.8)$$

where S_{Real} and ψ_R are the phase and wavefunction associated with the real branch, and S_{Sec} and ψ_S correspond to the secondary branch. In figures 2(a), 2(b) and 2(c) we compare the exact wavefunction with the numerical results obtained by applying CTM using a two-branch superposition. The figures indicate that when the wavefunction does not exhibit oscillations, the contribution of the real branch is sufficient to obtain a good approximation to the wavefunction. But at intermediate times, when the wavefunction exhibits interference effects, the contribution of both branches must be included. This last observation applies in the spatial range up to the classical turning point ($x \simeq 24$), beyond which the combined contribution diverges from the exact result.

We turn to a closer inspection of this divergence. In fig.3 we plot the contribution at $t_f = 6$ of each individual branch and their superposition. Starting from the vicinity of $x \simeq 22$, we observe an exponential increase of ψ_S . For $x \gtrsim 23$ we have a discontinuity of the approximation, as we discard the contribution of the secondary branch and include just the real branch. A description of this divergence appears in reference [19] in the context of the GGWPD formulation.

It is interesting to compare the time-dependence of the real and secondary branch contributions to the final approximation. A qualitative measure of the contribution of each branch is given by the imaginary part of the phase since

$$|\psi_R| = \left| \exp\left(\frac{i}{\hbar}S_{\text{Real}}\right) \right| = \exp\left[-\frac{\Im(S_{\text{Real}})}{\hbar}\right], \quad (3.9)$$

and a similar relation applies for ψ_S and $\Im(S_{\text{Sec}})$. In figures 4(a) and 4(b) we plot $\Im(S_{\text{Real}})$ and $\Im(S_{\text{Sec}})$ respectively for a series of final propagation times. We see that the secondary branch has a significant magnitude only at intermediate times. This observation coincides well with

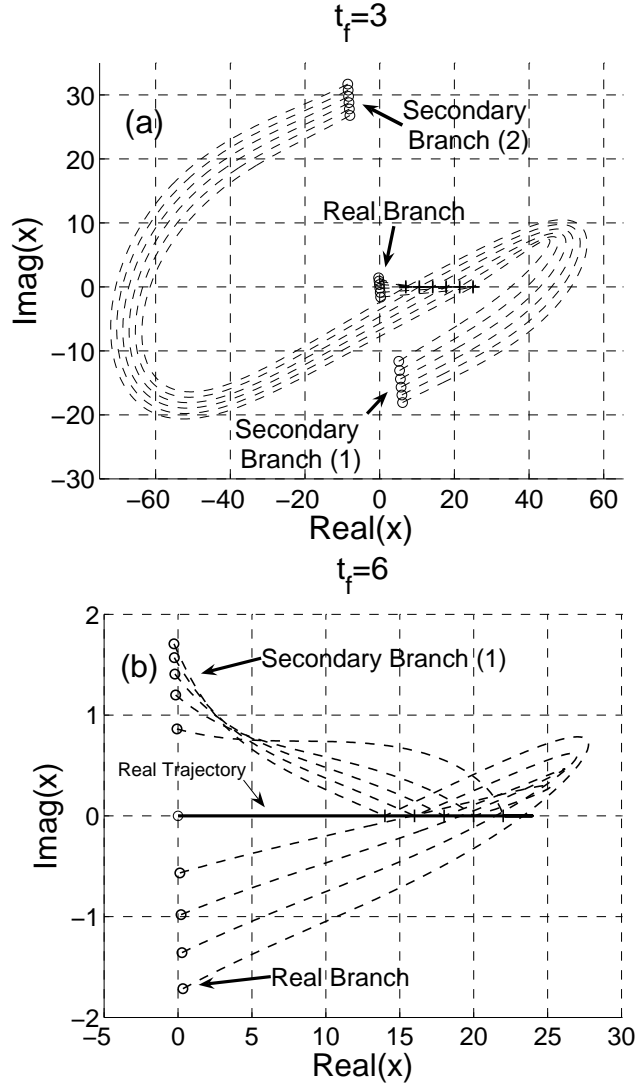


FIG. 1: Complex classical trajectories with initial positions marked as circles and *real* final positions (marked as pluses) at (a) $t_f = 3$ and (b) $t_f = 6$. The trajectories arise from an initial Gaussian wavepacket propagating in a quartic double-well potential. The Gaussian is centered at $x = 0$ and has positive initial momentum (the physical parameters are given in the text). In plot (a) we demonstrate that each final position arises from three initial positions. The initial positions are divided into a real branch and two secondary branches. The real branch is defined as incorporating a trajectory that remains on the real axis at all times. The real trajectory is specifically indicated in plot (b).

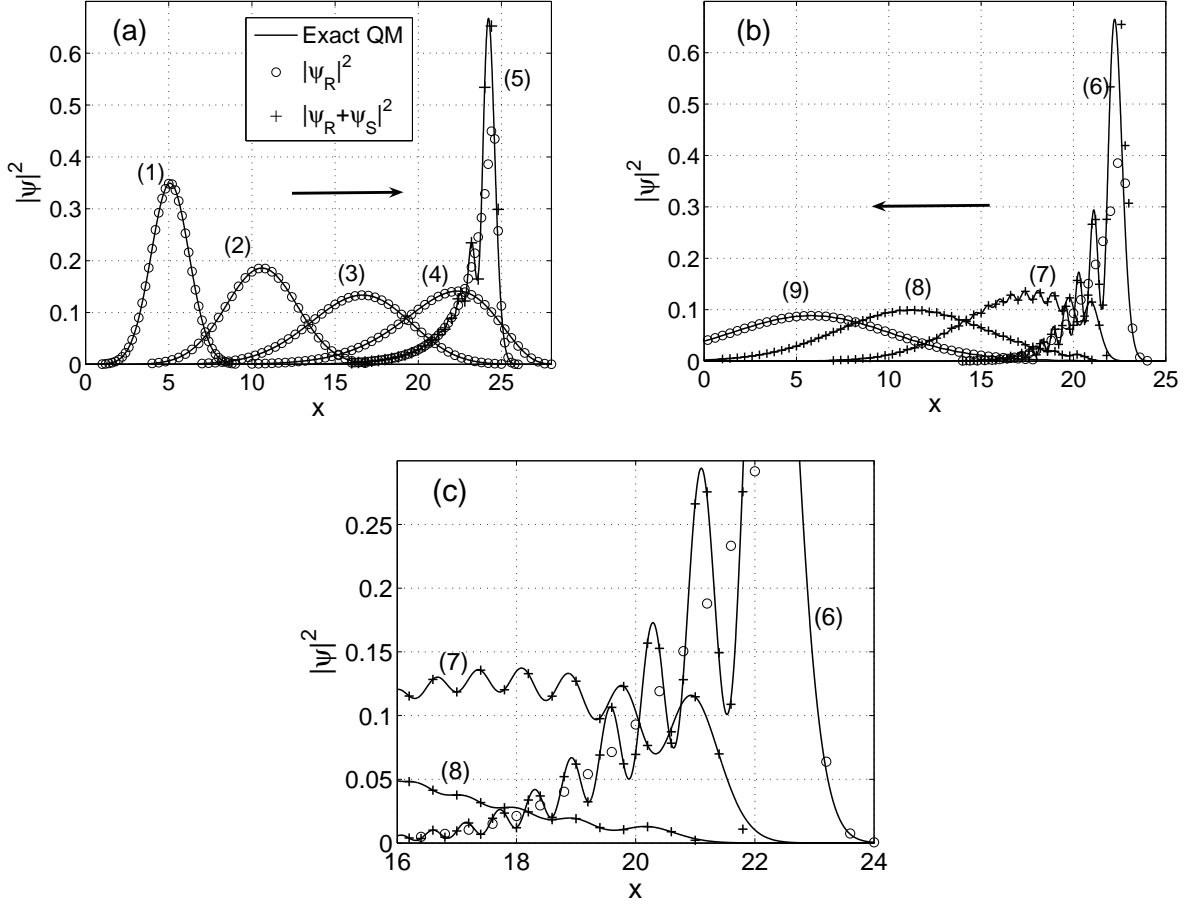


FIG. 2: A comparison between the exact quantum wavefunction and CTM ($N = 1$) with a two-branch superposition. The comparison is at a series of final propagation times specified by the numbers in the parentheses. The plots arise from an initial Gaussian wavepacket centered at $x = 0$ with a positive average momentum, propagating in a quartic double-well potential (the parameters are given in the text). (a) Initially right-propagating wavefunction; (b) the reflected wavefunction; (c) a zoom on a section of (b). For $t_f = 5$ in (a) and $t_f = 6$ in (b) and (c) we plot the results both for just the real branch $|\psi_R|^2$ and for the combination of branches $|\psi_R + \psi_S|^2$. The interference pattern obtained by superposing the contributions is clearly observed.

the need to include the contribution of the secondary branch to the final wavefunction only at these times. The exponential growth of ψ_S that is observed in fig.3 is also apparent in fig.4(b), in the negative parts of the graphs for $t_f = 5$ and $t_f = 6$. The divergent magnitude of ψ_S is in contrast to the finite magnitude of ψ_R that is observed in fig.4(a). A discontinuity

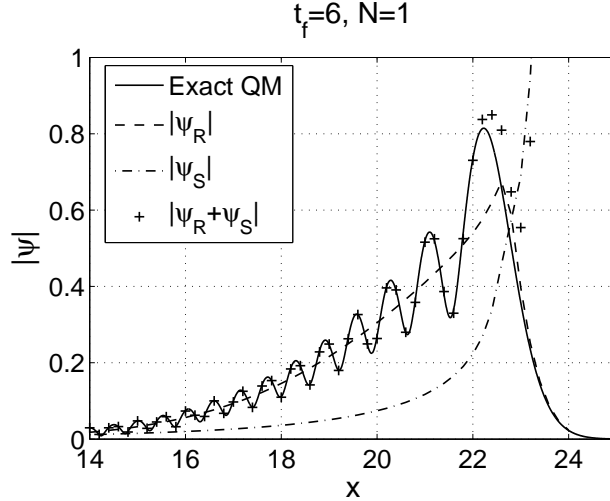


FIG. 3: CTM approximation at $t_f = 6$ for $N = 1$. The contributions of each branch to the wavefunction are depicted by plotting $|\psi_R|$, $|\psi_S|$ and $|\psi_R + \psi_S|$. Note the exponential increase of ψ_S begins around $x \simeq 22$. For $x \simeq 23$; we discard the contribution of the secondary branch and include just the real branch, leading to a discontinuity of the CTM approximation.

in the derivative of $\Im(S_R)$ at $t_f = 5$ and $t_f = 6$ is also observed. This discontinuity appears slightly prior to the points where the contribution of the secondary branch begins to diverge.

A close inspection of the complex trajectories at $t_f = 5$ and $t_f = 6$, reveals an interesting property of the real trajectory: the real trajectory acts as a boundary between two “regimes” of complex trajectories comprising from the real branch. This can be seen in fig.5, where the trajectories that initiate from $\Im[x(0)] > 0$ are seen to reach the real x -axis at values lower than the real trajectory while trajectories with $\Im[x(0)] < 0$ seem to go past the barrier and reach the real x -axis at values higher than the real trajectory. These two regimes correspond to the two legs of the “v”-shaped graph of $\Im(S_{\text{Real}})$ in fig.4(a): the trajectories arising from initial positions with $\Im[x(0)] > 0$ correspond to the left leg of the “v” while trajectories with $\Im[x(0)] < 0$ correspond to the right leg of the “v”.

B. Second Order approximation, $N = 2$

In this section we analyze the effect of incorporating S_2 in the CTM approximation. In addition to the five equations that are needed for obtaining the complex trajectories, S_0 and S_1 , we need to solve eqs.(2.22), (2.23) and (2.24). In fig.6(a) we depict the approximate wavefunction for $N = 2$ at $t_f = 6$. Comparing the $N = 2$ result with the $N = 1$ result plotted in fig.3, we conclude that other than an interval in the neighborhood of $x \simeq 22.5$, the $N = 2$ result (dashed line) lies on top of the exact result (solid line) and is significantly better than the $N = 1$ result. For $x \gtrsim 23$, where we incorporate solely the real branch contribution, the improvement in the approximation is graphically evident from the plots. For $x \leq 22$ we calculated the relative error between the absolute value of the approximations and the exact wavefunction using all the data points depicted in figs.3 and 6(a). The results are presented in fig.6(b). For $N = 1$ the mean relative error is 0.34% while for $N = 2$ the mean relative error is 0.11%. We see that the approximation worsens in the vicinity of the discontinuity of ψ_R . In the vicinity of $x \simeq 22.5$, the $N = 2$ results are worse than the $N = 1$ results; moreover, in the $N = 2$ case ψ_S as well as ψ_R exhibits a discontinuity.

IV. SUMMARY

In this paper we have presented a formulation of complex time-dependent WKB (CTDWKB) that allows the incorporation of interfering contributions to the wavefunction. The central idea in CTDWKB presented by Boiron and Lombardi[17] is to include both the amplitude and the phase in the lowest order term of the conventional time-dependent WKB method. The rationale behind this substitution is to treat the phase and the amplitude on equal footings in the limit $\hbar \rightarrow 0$. The benefits of the method are twofold. Firstly, CTDWKB exhibits accuracy superior to the conventional TDWKB[17]. Secondly, no singularities appear in the integration of the equations of motion. The method has two main *drawbacks*. First, the trajectories that emerge obey the classical equations of motion but propagate in the complex plane (due to complex initial conditions), requiring analytic continuation of the quantum wavefunction. The second drawback is that the reconstruction of the wavefunction on the real axis requires a root search process. This process can be eased by exploiting the analytic mapping between initial and final position.

We have incorporated into the CTDWKB method the possibility of contributions from multiple crossing trajectories. Boiron and Lombardi claim (section V in reference[17]) that they use the root search procedure “excluding de facto such double contributions”, although they appreciate the benefit that double contributions have in the GGWPD formulation. As we have demonstrated here, considering double contributions allows description of interference effects that are missing in the Boiron-Lombardi formulation of CTDWKB. Moreover, we have showed how to derive higher orders terms of the approximation in a straightforward manner. This process was applied for the derivation of a second order term in the CTDWKB approximation. The results for $N = 2$ were better than for $N = 1$ except for a small interval in the vicinity of the classical turning point. It was also observed that even though there are no singularities in the integration of the CTDWKB equations of motion, a singularity appears in the real branch ψ_R at intermediate times. For $N = 2$ an irregularity also appears in the part of the wavefunction associated with the secondary branch ψ_S . We demonstrated that when a singularity appears in ψ_R (at intermediate times), the real trajectory acts as the boundary between two groups of trajectories associated with the real branch. Each of these groups contributes to a different side of the singularity.

The CTDWKB formulation has several issues that require more comprehensive study. The most critical issue is to give an analytic explanation of the need to include the contributions from multiple classical trajectories (with zero relative phase) and why in some cases these contributions diverge. This will be dealt with in our forthcoming publication [22]. Some insight into the analytic structure of the complex classical trajectories was given in reference [19] in the context of GGWPD; however, we believe that a more general understanding of this structure is yet to be developed. This structure presumably is relevant to the question of when the CTDWKB formulation converges to the exact quantum mechanical result. We saw that in most parts of configuration space $N = 2$ performed better than $N = 1$, but in other parts of configuration space, where there were singularities, $N = 2$ performed worse. What determines the position and time-dependence of these singularities in ψ_R at intermediate times? What is the relation between the singularities in CTDWKB vs. conventional time-dependent WKB? Is there any fundamental limitation on the time scale for which the method is accurate? Since WKB plays such a central role in quantum mechanics in general and in semiclassical mechanics in particular, we believe that these questions are of great general interest. The developments described in this paper together with the

answers to some of the above questions could make the time-dependent WKB formulation a competitive alternative to current time-dependent semiclassical methods.

We wish to acknowledge David Kessler and Uzi Smilansky for useful discussions. This work was supported by the Israel Science Foundation (576/04).

-
- [1] G. Wentzel, *Z. Phys.* **38**, 518 (1926).
 - [2] H. A. Kramers, *Z. Phys.* **39**, 828 (1926).
 - [3] L. Brillouin, *CR Acad. Sci, Paris* **183**, 24 (1926); L. Brillouin, *J. Phys.*, **7**, 353 (1926)
 - [4] W. Pauli, *Die allgemeine Prinzipien der Wellenmechanik*, Encyclopedia of Physics, Vol. 5, Springer, Berlin, 1958.
 - [5] K. Gottfried, *Quantum Mechanics, Volume I: Foundations* (W. A. Benjamin, New York, 1966)
 - [6] Byung Chan Eu, *W. J. Chem. Phys.* **57**, 2531 (1972).
 - [7] H. J. Korsch, R. Mohlenkamp, *Phys. Lett. A* **67**, 110 (1978).
 - [8] S. M. Blinder, *Chem. Phys. Lett.* **137**, 288 (1987).
 - [9] L. Raifeartaigh, A. Wipf, *Found. Phys. Lett.* **18**, 307 (1987).
 - [10] M. P. A. Fisher, *Phys. Rev. B* **37**, 75 (1988).
 - [11] R. Rubin, Junior paper (Princeton, 1990).
 - [12] M. Burdick, H. J. Schmidt, *J. Phys. A: Math. Gen.* **27**, 579 (1994).
 - [13] C. Sparber, P. A. Markowich, N. J. Mauser, arXiv:math-ph/0109029 (2002).
 - [14] A. S. Sanz, F. Borondo, S. Miret-Artés, *J. Phys.:Condens. Matter* **14**, 6109 (2002).
 - [15] Jeong Ryeol Choi, *Int. J. Theo. Phys.* **43**, 947 (2004).
 - [16] P. Bracken, arXiv:math-ph/0608011v2 (2006).
 - [17] M. Boiron, M. Lombardi, *J. Chem. Phys.* **108**, 3431 (1998).
 - [18] D. Huber, E. Heller, *J. Chem. Phys.* **87**, 5302 (1987).
 - [19] D. Huber, E. Heller, R. G. Littlejohn, *J. Chem. Phys.* **89**, 2003 (1988).
 - [20] Y. Goldfarb, I. Degani, D. J. Tannor, *J. Chem. Phys.* **125**, 231103 (2006).
 - [21] Y. Goldfarb, D. J. Tannor, submitted.
 - [22] J. Schiff, Y. Goldfarb, D. J. Tannor, in preparation.

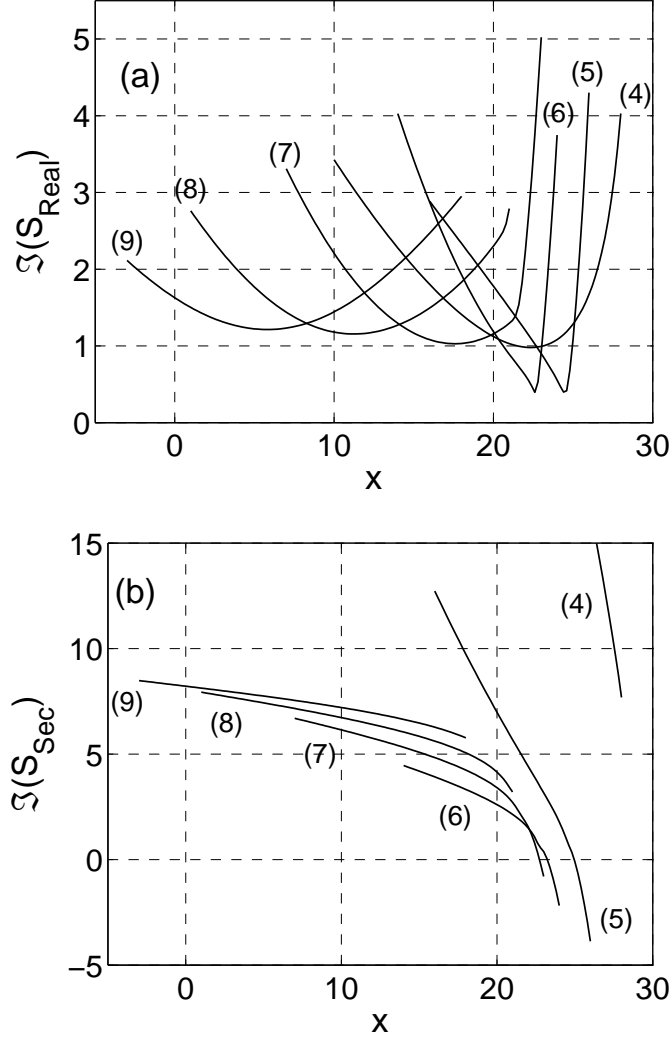


FIG. 4: (a) $\Im(S_{\text{Real}})$ and (b) $\Im(S_{\text{Sec}})$ are depicted at a series of final propagation times (given in the parentheses). The results are limited to the spatial interval for which the absolute value of the exact wavefunction is significantly larger than zero. The imaginary part of the phase allows for a qualitative estimate of the contribution of each branch to the probability $|\psi_{\text{R}} + \psi_{\text{S}}|^2$, see eq.(3.9). Figure (b) shows that $\Im(S_{\text{Sec}})$ drops below ~ 2 only for a finite interval of intermediate times. Therefore only for this range of times does the secondary branch makes a significant contribution to the wavefunction.

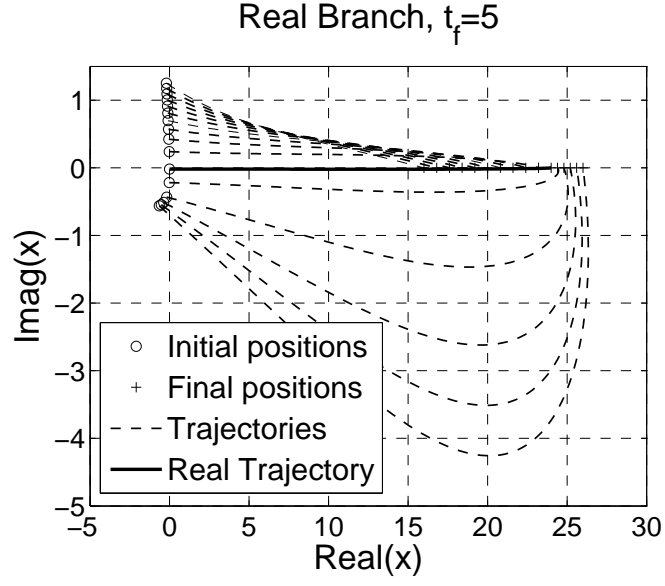


FIG. 5: Complex classical trajectories that correspond to the *real branch* at $t_f = 5$. The real trajectory acts as a boundary between two “regimes” of the complex trajectories. Initial positions with $\Im[x(0)] < 0$ seem to be go past the potential wall. The two “regimes” can be related to the singular behavior of the derivative of $\Im(S_{Real})$ at intermediate times (fig.4(a)).

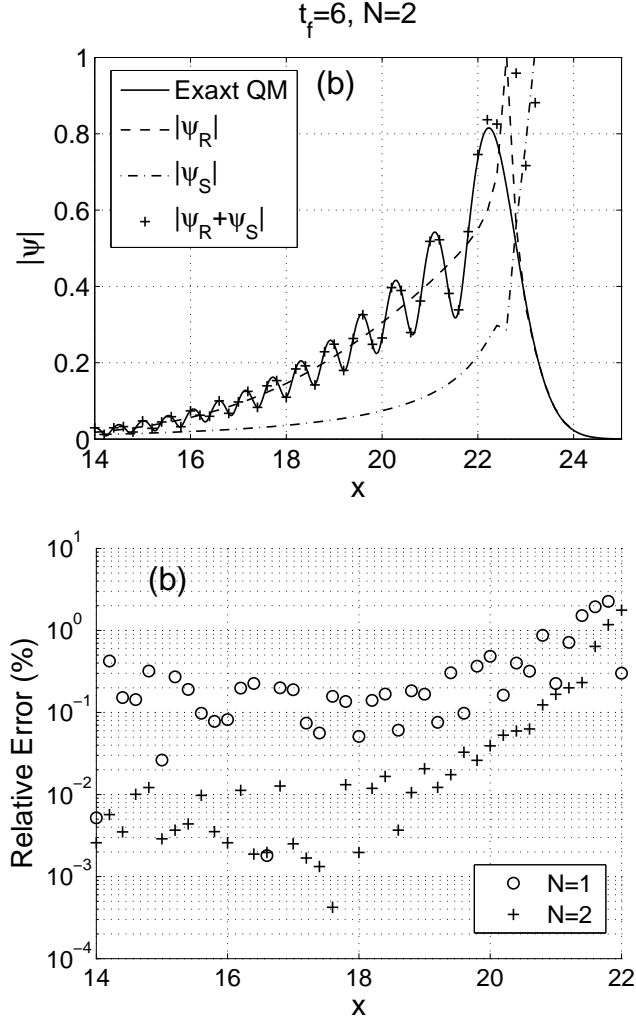


FIG. 6: (a) The second order ($N = 2$) CTM approximation is depicted for $t_f = 6$. A discontinuity appears at $x \simeq 22.5$ for both ψ_R and ψ_S . (b) The relative error between the absolute value of the exact quantum wavefunction and the CTM approximation for $N = 1$ and $N = 2$, based on the data in fig.3 and fig.6(a). A comparison of the relative errors indicates a clear improvement when taking an additional order in the CTM approximation.